Bioprospecting of Zinc Oxide Nanoparticles from *Bacillus subtilis* subsp. *subtilis* HSFI-9 Extract: Unveiling Their Potential as Antibacterial Agents

Maya Dian Rakhmawatie[1], Ana Hidayati Mukaromah[2], Ika Dyah Kurniati[1], Nur Fadhila Sari[3], Mazidatu Khoirinnisa Adiyanti[3], and Arman Suryani[4*]

[1]*Department of Biomedical Sciences, Faculty of Medicine, Universitas Muhammadiyah Semarang, Semarang 50273, Indonesia*

[2]*Department of Chemistry, Magister Study Program of Clinical Laboratory Science, Universitas Muhammadiyah Semarang, Semarang 50273, Indonesia*

[3]*Medical Student, Faculty of Medicine, Universitas Muhammadiyah Semarang, Semarang 50273, Indonesia*

[4]*Department of Pharmacy Undergraduate Studies, Faculty of Pharmacy, Sultan Agung Islamic University, Semarang 50112, Indonesia*

Corresponding author:

tel: +62-85257511518
email: arman.s@unissula.ac.id

Received: October 30, 2025
Accepted: January 15, 2026

DOI: 10.22146/ijc.112650

Abstract: Bacillus subtilis *subsp.* subtilis *HSFI-9 demonstrates the ability to inhibit bacterial growth* in vitro*, with the potential for enhancement through nanoparticle technology. This study innovatively impregnated ZnO-NPs into the HSFI-9 extract to optimize its antibacterial activity, using the precipitation method with zinc nitrate tetrahydrate precursor at pH 10.0. Antibacterial tests were conducted against* Acinetobacter baumannii, Enterococcus faecium, Enterobacter aerogenes, Klebsiella pneumonia, Pseudomonas aeruginosa, *and* Staphylococcus aureus *using the disc diffusion and microdilution methods. Physical and chemical characterizations of ZnO-NPs HSFI-9 were also performed, and secondary metabolites were analyzed using high-resolution mass spectroscopy. The results revealed that ZnO-NPs HSFI-9 showed moderate antibacterial activity against* S. aureus *(MIC: 97.6 µg/mL),* K. pneumoniae*, and* E. aerogenes *(MIC: 390.6 µg/mL). SEM-EDX analysis showed particle sizes of 185–189 nm, with a hexagonal-spherical morphology. DLS measurements indicated larger particle sizes in the micrometer range because it measured the hydrodynamic diameter, which includes the solvent layer, whereas SEM measures individual particle size based on physical appearance. The crystallinity index of ZnO-NPs HSFI-9 was 67.3% based on XRD analysis. Surfactin was the primary metabolite detected in the extract, suggesting positive prospects for developing ZnO-NPs HSFI-9 as an antimicrobial agent.*

Keywords: *antibacterial agents;* Bacillus subtilis*;* Staphylococcus aureus*; zinc oxide nanoparticles*

■ INTRODUCTION

Bacillus subtilis subsp. *subtilis* HSFI-9, hereinafter referred to as HSFI-9, is known to have the ability to inhibit the growth of several pathogenic bacteria. The ethyl acetate extract produced by HSFI-9 is known to contain the volatile compound 1-butanol, 3-methyl-formate from the gas chromatography-mass spectroscopy (GC-MS) profile, which is presumed to be the compound that determines its antibacterial activity. This potential is not yet supported by optimal extract production capacity (only around 24 mg/L of culture) [1-2]. Low extract production capacity can increase costs; therefore, optimization is needed to improve the efficiency of antibacterial drug development from HSFI-9. The HSFI-9 was chosen for this study due to its proven ability to inhibit bacterial growth, particularly against major pathogenic bacteria such as *Staphylococcus aureus*, *Klebsiella pneumoniae*, and *Enterobacter aerogenes*. The HSFI-9 extract contains bioactive compounds, including

surfactin, which are believed to contribute to its antimicrobial activity.

One approach to enhance its effectiveness is by impregnating the extract with metal nanoparticles, such as zinc oxide nanoparticles (ZnO-NPs), which can strengthen its antibacterial activity. Metal-impregnated nanoparticles are known to possess antimicrobial properties effective against a wide range of microorganisms, including bacteria, fungi, and viruses [3-4]. This advantage makes HSFI-9 distinct from other Bacillus strains, making it an excellent choice for the development of more efficient antimicrobial agents. Impregnation of metal nanoparticles can be used to optimize the antibacterial activity of the extract [5-6]. Metal-impregnated nanoparticles are known to have antimicrobial properties against bacteria, fungi, or viruses. The combination of nanoparticles with antibiotics has also been widely studied regarding the synergy of effects and increased ability to reduce antibiotic resistance [3-4].

Inorganic compounds such as ZnO have been known as a nanoparticle impregnation material that is useful for increasing the antimicrobial activity of plant extracts or antibiotics. ZnO-NPs have the advantage of requiring low costs for the manufacturing process [7]. Topical ZnO-NPs are also known to accelerate re-epithelialization and eliminate lesions caused by topical skin infections [8]. For example, successful ZnO impregnation of ketoconazole can increase penetration and accumulation of ketoconazole in the skin [9]. ZnO-NPs also have advantages such as low toxicity [10], although if it is used for a long period can accumulate in tissues and cause skin sensitization reactions [11].

The biosynthesis of ZnO-NPs with microbial secondary metabolites has been widely studied. Secondary metabolites of *Trichoderma* sp. were successfully impregnated with Zn to produce hexagonal/spherical nanoparticle molecules with a size of 8–30 nm [12]. ZnO-NP biosynthesis was also successfully carried out on secondary metabolites of *Streptomyces* sp. and *Bacillus* sp., with particle size results of 20–95 nm [13]. Several studies related to impregnation of ZnO-NPs from secondary metabolites of *Bacillus* sp. have been conducted, including *Bacillus foraminis* which produces spherical particle shapes, but there is no information regarding its activity [14], or ZnO-NPs of *B. subtilis* which produces activity as a nano fertilizer [15]. One of the nanoparticles that has been successfully produced has antibacterial activity against *Escherichia coli* and *S. aureus* was ZnO-NPs of *Bacillus haynesii* [16].

Research on ZnO-NPs has been extensively conducted for antibacterial applications. ZnO-NPs are known to be effective against a wide range of pathogens, including both Gram-positive and Gram-negative bacteria. For instance, a study by Gudkov et al. [7] demonstrated that ZnO-NPs exhibit antibacterial activity against *E. coli* and *S. aureus*. However, studies focusing on the impregnation of ZnO-NPs into microbial extracts, such as the one conducted on *B. subtilis* subsp. *subtilis* HSFI-9, remain limited. Most previous studies by Rehman et al. [16], and El-Ghwas [14], focused more on the biosynthesis of ZnO-NPs using *Bacillus* strains like *B. haynesii* and *B. foraminis*, but no research has specifically explored the antibacterial potential of ZnO-NPs impregnated with *B. subtilis* subsp. *subtilis* HSFI-9 extract. The impregnation of ZnO into HSFI-9 extract has not been previously done; therefore, this study aims to optimize the antibacterial activity of ZnO-NP HSFI-9. The antibacterial activity was tested against various skin infection pathogens, such as *Acinetobacter baumannii*, *Enterococcus faecium*, *Enterobacter* sp., *K. pneumoniae*, *Pseudomonas aeruginosa*, and *S. aureus* (ESKAPE), which are known to have high antibiotic resistance levels [17]. The physical and chemical properties of ZnO-NP HSFI-9 were evaluated by analyzing the ZnO vibration spectrum at 500–600 cm^{-1} using Fourier transform-infrared spectroscopy (FTIR) [18]. The particle size, distribution, and aggregation level of ZnO-NP HSFI-9 were tested using dynamic light scattering (DLS) to ensure that the particle size falls within the range of 5–100 nm [19]. The three-dimensional shape, crystal structure, and elemental composition were analyzed through X-ray diffractometry (XRD) and scanning electron microscopy-energy dispersive X-ray (SEM-EDX) [20]. Additionally, the secondary metabolite profile of the HSFI-9 extract was further analyzed using

liquid chromatography-high resolution mass spectrometry (LC-HRMS) [21]. While many studies indicate synergy between nanoparticles and antibiotics in enhancing antibacterial activity [4], there is still a gap in knowledge regarding the specific action mechanism of nanoparticles impregnated with microbial extracts. Furthermore, the limited production capacity of the HSFI-9 extract, about 24 mg/L, reduces efficiency and increases production costs, thus requiring optimization to enhance the effectiveness of antibacterial drug development from HSFI-9. This study aims to fill this gap by optimizing the antibacterial activity of HSFI-9 extract through ZnO-NP impregnation and further investigating the antibacterial mechanisms involved, particularly against multi-drug-resistant pathogens such as *A. baumannii* and *S. aureus*.

■ EXPERIMENTAL SECTION

Materials

All materials used in this study were reagent grade (98–99%), before being diluted according to test requirements. Starch, sodium chloride (NaCl), zinc nitrate hexahydrate ($Zn(NO_3)_2{\cdot}6H_2O$), sodium hydroxide (NaOH), Mueller Hinton agar (MHA), Mueller Hinton Broth (MHB), potassium bromide (KBr), and methanol were supplied from Merck. Yeast and peptone used in this study were from BD Difco, and dimethyl sulfoxide (DMSO) from Sigma Aldrich.

Instrumentation

The instruments used in nanoparticle synthesis were a hotplate stirrer (Ika®) and an oven (Binder GmbH). FTIR analysis was performed using an instrument from Thermo Scientific (Nicolet iS-10). Particle size distribution was measured using the DLS method (Malvern, ZS Nano, UK) and a cuvette (DST 1070). The morphology, size, and element composition of biosynthesized ZnO-NPs HSFI-9 were determined using SEM-EDX (JSM-6510LA). The size and crystallinity of ZnO-NPs HSFI-9 were determined using the XRD analysis (Bruker AXS D8 Advance). Metabolites profiling from the HSFI-9 extract was performed using HR-MS, UHPLC (Thermo Scientific™ Ultimate™ 3000 RSLCnano).

Procedure

HSFI-9 extract production

Extract production was carried out by culturing HSFI 9 with 1L of nutrient media containing starch, yeast, peptone (SYP), and 0.5% NaCl. Culture and extraction methods were carried out according to previous research [2].

ZnO-NPs HSFI-9 production

The chemical synthesis of ZnO-NPs was carried out using the co-precipitation method. First, 0.2 M $Zn(NO_3)_2$ in 50 mL of water was stirred at 60 °C for 5 min. Next, a 5 M NaOH solution was slowly added to the $Zn(NO_3)_2$ solution until the pH reached 10.0. The resulting mixture was continuously stirred at 600 rpm at 60 °C for 2 h, producing a milky white solution. The precipitation process was then allowed to continue for 48 h at room temperature in a dark place. Afterward, the precipitate was centrifuged at 2000 rpm for 10 min, and impurities were removed by washing with water [22]. The ZnO-NPs were dried at 80 °C in an oven for 24 h. Once dried, the ZnO-NPs were ground to a fine powder before being stored in glass bottles. For the synthesis of ZnO-NPs HSFI-9, the same method was used as for the ZnO-NPs, with the addition of 25 mL of HSFI-9 extract (3% w/v) after the $Zn(NO_3)_2$ solution had been conditioned to pH 10.0. The mixture was stirred at 60 °C for 1 h to ensure uniform distribution of the ZnO-NPs and HSFI-9 extract. This impregnation process was designed to enhance the antibacterial activity of the HSFI-9 extract incorporated into the ZnO-NPs. The aim of impregnating HSFI-9 into the ZnO-NPs was to optimize the antibacterial efficacy of the extract by leveraging the synergistic properties of ZnO-NPs and the bioactive components present in the HSFI-9 extract [23-24].

Antibacterial activity tests of ZnO-NPs HSFI-9

Antibacterial activity was tested on *A. baumannii* (ATCC 17978), *Enterococcus faecalis* (ATCC 29212), *E. aerogenes* (ATCC 13048), *K. pneumoniae* (ATCC 700603), *P. aeruginosa* (ATCC 9027), and *S. aureus* (ATCC 6538). The bacterial suspension was adjusted to a density equivalent to the McFarland standard 0.5. After inoculating the bacteria onto the MHA surface

using a sterile cotton swab, 50 µg of HSFI-9, ZnO-NP, and ZnO-NP HSFI-9 extracts were placed onto 6 mm blank discs, which were then positioned on the MHA surface. The Petri dishes were incubated at 37 °C for 18 h (for *E. faecalis*, *S. aureus*, *P. aeruginosa*, and *E. aerogenes*) or 24 h (for *K. pneumoniae* and *A. baumannii*). The antibacterial activity tests were performed in triplicate (n = 3) to ensure reproducibility and reliability of the results. A negative control was included by placing discs containing only DMSO onto the MHA surface to ensure that any observed antibacterial activity was not due to the solvent. The control antibiotic activity tests were performed using meropenem (10 µg) for *K. pneumoniae*, *A. baumannii*, *P. aeruginosa*, and *E. aerogenes*, or co-amoxiclav (30 µg) for *E. faecalis* and *S. aureus* to confirm that the bacterial isolates tested were sensitive to antibiotics. The inhibition zones were measured using a caliper to determine the extent of microbial growth inhibition [25-26]. The microdilution activity test was carried out using a two-fold dilution method with concentrations ranging from 2500.0 to 39.0625 µg/mL for the HSFI-9 extract, except for *S. aureus* (two-fold dilution up to 1.22 µg/mL). For ZnO-NPs and ZnO-NP HSFI-9, the concentration range was from 6250.0 to 24.414 µg/mL. The final concentration of the bacterial suspension in the microplate was adjusted to 1.75×10^5 CFU/mL. Antibiotic controls used included ampicillin at a maximum concentration of 32.0 µg/mL for *E. faecalis* and *S. aureus*, or ceftazidime at a maximum concentration of 32.0 µg/mL for the other bacteria. The plates were incubated at 37 °C for 18–24 h, and the results were interpreted using resazurin staining [1]. All inhibition zone diameters and MIC values were statistically analyzed using one-way analysis of variance (ANOVA), followed by Tukey's post hoc test to identify significant differences among treatments. A p-value of less than 0.05 was considered statistically significant, and such differences were indicated by an asterisk (*).

ZnO-NPs HSFI-9 physicochemical evaluation using FTIR, Particle Size Analyzer (PSA), SEM-EDX, and XRD

Functional group spectra of the ZnO-NPs HSFI-9 were measured using FTIR. The ZnO-NPs HSFI-9 was compressed into KBr pellets using a hydraulic pressure of 5 tons for 5 min. The discs were measured at a wavelength of 400–4000 cm^{-1} [27]. The particle size distribution was analyzed by taking 3 mL of ZnO-NPs HSFI-9 solution that had been previously dissolved in methanol. The ZnO-NPs HSFI-9 solution in methanol was sonicated before being put into a cuvette to measure the droplet size. Measurements were carried out three times, along with the zeta potential value [28-29].

Analysis using SEM-EDX was performed by pouring ZnO-NPs onto a glass object and then allowing them to dry before placing them in the tool. Results reading is carried out with a voltage of 15 kV and magnifications of 5000, 10000, 15000, 20000, and 30000. The ZnO-NPs size stipulation was assessed using SEM micrographs [30]. The size and crystallinity of ZnO-NP HSFI-9 were analyzed using XRD. The sample was placed on a glass slide with a Bragg angle ranging from 20° to 100°. XRD was employed to determine both the particle size and crystallinity index of the nanoparticles. The particle size was calculated using the Debye-Scherrer (Eq. (1)) [30];

$$D = \frac{K\lambda}{\beta \cos\theta} \quad (1)$$

where D represents the particle size, K is the shape factor of the crystal, λ is the X-ray wavelength, β is the full width at half maximum (FWHM) of the X-ray peak, and θ is the Bragg angle. The crystallinity index was determined from the intensities of the main diffraction peaks, which help assess the degree of order in the nanoparticle crystal structure. This method provides valuable insights into the stability and ordering of the ZnO-NP HSFI-9 crystals, which is crucial for understanding the nanoparticle's crystallographic characteristics [30].

Secondary metabolites profiling of HSFI-9 extract

Profiling secondary metabolites of the HSFI-9 extract was carried out using targeted and untargeted UHPLC-HRMS. The method used refers to previous studies with modifications in the addition of heated ESI (−) scans [31].

■ RESULTS AND DISCUSSION

Antibacterial Activity of ZnO-NPs HSFI-9

The results from the disk diffusion assay showed that ZnO-NPs derived from HSFI-9 produced a larger

inhibition zone against *S. aureus* compared to the HSFI-9 extract. However, the microdilution assay revealed that the minimum inhibitory concentration (MIC) for ZnO-NPs HSFI-9 was higher (97.6 μg/mL) than that of the crude extract (1.22 μg/mL). This difference can be attributed to the lower proportion of bioactive components from HSFI-9 incorporated into the ZnO-NP matrix during synthesis, with only about 3% of the active extract included. As a result, the increased MIC is a natural consequence of the reduced concentration of the bioactive extract in the nanoparticle formulation. The observed increase in MIC is considered normal due to the dilution effect of the extract within the nanoparticle matrix. The small proportion of extract incorporated into the ZnO-NP formulation results in a lower concentration of active bioactive compounds, which naturally leads to a higher MIC. Despite this, the antibacterial activity remains intact, thanks to the synergistic effects between the ZnO-NPs and the bioactive compounds from the extract. Thus, although the MIC value is higher, the antibacterial activity of ZnO-NP HSFI-9 remains significant. This outcome is typical when formulating nanoparticle-based systems, where the bioactive components may be diluted but still contribute to the overall antimicrobial effect. Further optimization of the formulation could improve the antibacterial efficacy of ZnO-NP HSFI-9 [32-33]. Additionally, the small amount of extract used during synthesis was deliberately chosen to maximize material efficiency, given its limited availability and high production cost.

The variation in maximum concentrations used in the MIC testing was based on the solubility profiles and activity ranges of the different test materials. For the HSFI-9 extract, concentrations were tested within a range of 2500.0 to 39.0625 μg/mL (except for *S. aureus*, which was tested up to 1.22 μg/mL), to evaluate its effectiveness within a clinically relevant concentration range. In contrast, ZnO-NPs and ZnO-NP HSFI-9 were tested at higher concentrations, ranging from 6250.0 to 24.414 μg/mL. This difference in concentration was due to the distinct characteristics of the nanoparticle formulations, which generally require higher doses to produce effective inhibition due to their larger particle size and lower bioavailability in solid form. These concentrations to validate the results and rule out any potential interference from the solvent, a negative control was included in the study. Discs containing only DMSO were placed on the MHA surface alongside the experimental discs containing the HSFI-9 extract, ZnO-NPs, and ZnO-NP HSFI-9. The control discs did not produce any inhibition zones, confirming that the antibacterial effects observed were carefully selected to ensure that each material was tested within its optimal and applicable dose range to evaluate its potential antibacterial activity. Furthermore, the solubility of the nanoparticles in the testing medium was also considered, as nanoparticles tend to have lower solubility compared to the extract, thus necessitating higher concentrations to achieve similar effects. attributed to the active compounds in the nanoparticle formulations rather than the solvent.

According to Table 1, ZnO-NPs HSFI-9 exhibited overall higher antibacterial activity than the HSFI-9

Table 1. Recapitulation of mean and standard deviations of the ZnO-NP of the ethyl acetate extract of *B. subtilis* subsp. *subtilis* HSFI-9 activity test results against tested bacteria using the disc diffusion and microdilution test

Tested bacteria	Inhibition zone from disc diffusion (mm)			MIC from microdilution (μg/mL)		
	HSFI-9	ZnO-NP	ZnO-NP HSFI-9	HSFI-9	ZnO-NP	ZnO-NP HSFI-9
E. faecalis	1.67 ± 0.58	-	-	156.25	-	-
S. aureus	15.00 ± 1.00	-	17.33 ± 0.58*	1.22	390.60	97.60
K. pneumoniae	-	ND	ND	-	781.25	390.60
A. baumannii	2.33 ± 0.58	-	1.00 ± 0.00*	156.25	-	-
P. aeruginosa	-	ND	ND	-	6250.00	6250.00
E. aerogenes	-	ND	ND	-	3125.00	390.60

Note: Dosage per disc for HSFI-9, ZnO-NP, and ZnO-NP HSFI-9 were 50 μg; (ND) not determined; (-) no inhibition; maximum concentration of ZnO-NPs for microdilution was 6250 μg/mL; *significantly different

extract but remained lower than pure ZnO. These findings imply that extract-derived compounds entrapped within the nanoparticle matrix contribute to antibacterial activity, although their low concentration prevents them from fully reaching the effectiveness of ZnO alone. Such conditions merit further evaluation, particularly concerning the potential role of bioactive compounds as supportive but non-dominant contributors when integrated into nanoparticle structures. It is also notable that, despite reduced activity against S. aureus as indicated by MIC values, ZnO-NPs HSFI-9 demonstrated improved inhibitory effects against *K. pneumoniae* and *E. aerogenes*.

Importantly, the relatively weak antibacterial response of ZnO-NPs in disk diffusion assays is likely attributable to the solid physicochemical properties of nanoparticles, which limit their diffusion through the agar matrix. Poor solubility restricts their antibacterial action primarily to the area in direct contact with bacterial cells, resulting in a comparatively narrow inhibition zone. Furthermore, the antibacterial mechanism of ZnO-NPs typically requires direct cell particle interaction and reactive oxygen species (ROS) generation, both of which occur more efficiently in liquid media, as in the microdilution assay. Therefore, these conditions may explain the more pronounced antibacterial performance of ZnO-NPs observed in microdilution compared with disk diffusion testing [34-35].

The antibacterial mechanism of ZnO-NPs HSFI-9 is presumed to be primarily associated with the enhanced generation of ROS resulting from the interaction of released Zn^{2+} ions with bacterial cells. This process can disrupt enzymatic and respiratory functions, ultimately leading to protein denaturation and DNA damage. In addition, ZnO-NPs are reported to induce direct disruption of the bacterial cell membrane, further contributing to their bactericidal activity. Several studies have documented that ZnO-NPs exert antibacterial effects against both Gram-positive and Gram-negative bacteria [7]. Increased susceptibility of Gram-positive species is likely related to their cell wall architecture, which consists mainly of peptidoglycan and teichoic acids and exhibits higher porosity, facilitating nanoparticle penetration. In contrast, the outer membrane of Gram-negative bacteria composed of phospholipids, lipopolysaccharides, and lipoproteins, may act as a physical barrier that limits nanoparticle entry [36].

ZnO-NPs HSFI-9 Physicochemical Evaluation Using FTIR, PSA, SEM-EDX, and XRD

The synthesis of ZnO-NPs from the HSFI-9 extract using the co-precipitation method follows a bottom-up approach, where nanoparticles are formed from simpler precursors. In this approach, a chemical reaction facilitates nucleation and subsequent particle growth through a precipitation process, where atoms or molecules gather to form structures at the nanometer scale. The success of the bottom-up synthesis method depends heavily on precise control of experimental variables, including pH, temperature, and the presence of stabilizing or complexing agents. This method enables the production of nanoparticles with better homogeneity and improved physicochemical stability. Previous studies have shown that a pH of 10 results in different crystal sizes and optical properties compared to other pH values, indicating that pH significantly influences the physical characteristics of ZnO-NPs. At lower or higher pH levels, the size and morphology of the particles may change, which affects their optical properties and antibacterial activity [24]. Therefore, pH 10 is often selected as the optimal condition for synthesis to achieve the desired particle size and crystal structure. Proper pH control allows for better management of the morphology and crystallinity of ZnO-NPs, which is crucial in antibacterial applications, where particle stability and effectiveness must be optimized. In this study, the co-precipitation method provides greater control over the particle size and crystalline structure of the resulting ZnO-NPs, enabling the synthesis of well-defined, uniform nanomaterials suitable for antibacterial applications.

ZnO-NPs HSFI-9 exhibited a decrease in the transmittance peak intensity at wavelengths of 447–452, 882, and 3451 cm^{-1} (Fig. 1). In general, the peak patterns between ZnO-NPs and ZnO-NPs HSFI-9 are not different. Peaks around 882 and 1400 cm^{-1} indicate the

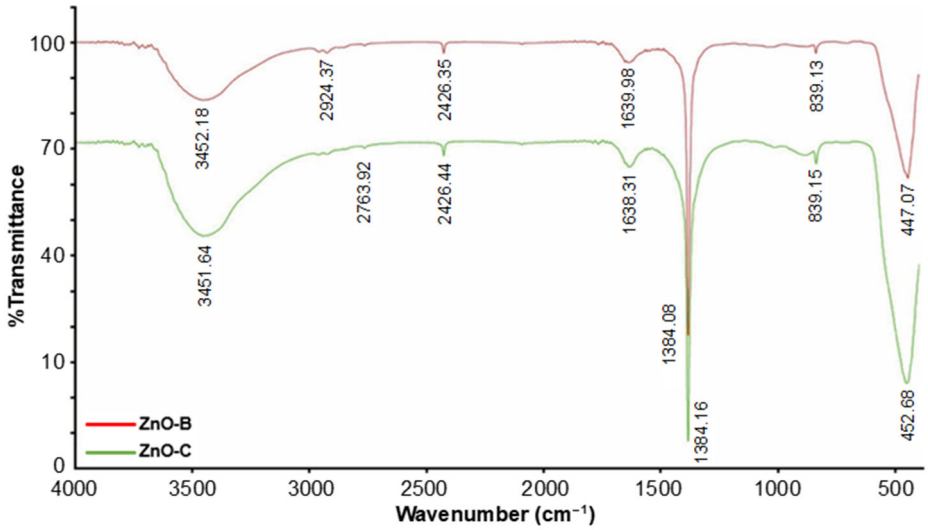


Fig 1. Overlay spectra Fourier transformed-infra red of ZnO-NPs (green line) and ZnO-NPs HSFI-9 (red line)

absorption of inorganic carbonate compounds. The peak around 3451 cm^{-1} shows changes in the stretching vibration of the alcohol. The peak area at around 450 cm^{-1} is the fingerprint area, in this case the ZnO-NPs stretching area, while ZnO stretching can be seen from the transmittance peak at 1639 cm^{-1} [37].

Particle size analysis was performed using SEM with magnifications ranging from 5,000× to 30,000× (Fig. 2). A minimum of 100 particles were randomly selected from different areas of the sample to determine the particle size distribution, and a histogram of the particle size distribution was constructed to evaluate the uniformity of the nanoparticle sizes [38]. The analysis revealed that ZnO-NPs HSFI-9 possessed smaller particle sizes compared with conventional ZnO-NPs, along with lower polydispersity index and zeta potential values (Table 2), indicating a narrower and more homogeneous particle size distribution. These findings suggest that the HSFI-9 extract acted as an effective stabilizing agent during synthesis, preventing particle agglomeration and improving size control. Although the particle size of ZnO-NPs HSFI-9 was smaller, no substantial difference was observed in the average crystallite size between ZnO-NPs (54.02 ± 21.81 nm) and ZnO-NPs HSFI-9 (51.49 ± 21.02 nm). Nevertheless, the degree of crystallinity was higher in ZnO-NPs HSFI-9 (67.3%) compared with conventional ZnO-NPs (63.6%). This increase indicates that the HSFI-9 extract contributed to the formation of a more organized and stable ZnO crystalline structure, which may enhance its applicability in various fields, including antibacterial and photocatalytic applications. The XRD profiles of both types of nanoparticles exhibited characteristic diffraction peaks consistent with previously reported ZnO patterns, with the most intense peak detected at approximately 36°, confirming high crystallinity of the synthesized materials [39-40]. Both ZnO-NPs and ZnO-NPs HSFI-9 displayed ZnO diffraction peaks around 31°, 34°, 36°, 47°, 56°, 62°, 66°, 67°, 69°, 72°, 76°, 81°, 89°, 92°, 95°, and 98°, with the dominant reflection at approximately 36° (Fig. 3).

Table 2. Recapitulation of mean and standard deviation of dynamic light scattering parameter from ZnO-NPs of ethyl acetate extract of *B. subtilis* subsp. *subtilis* HSFI-9

ZnO-NP type	Weight of ZnO-NP (mg)	%HSFI-9 extract	Particle size (nm)*	Polydispersity index (PDI)	Zeta potential (mV)
ZnO-NP	953.3 ± 53.50	-	2235.7 ± 378.20	0.674 ± 0.129	−1.71 ± 0.89
ZnO-NP HSFI-9	931.5 ± 50.10	3.23 ± 0.18	1501.3 ± 130.70	0.409 ± 0.013	−29.01 ± 0.70

Note *significant difference

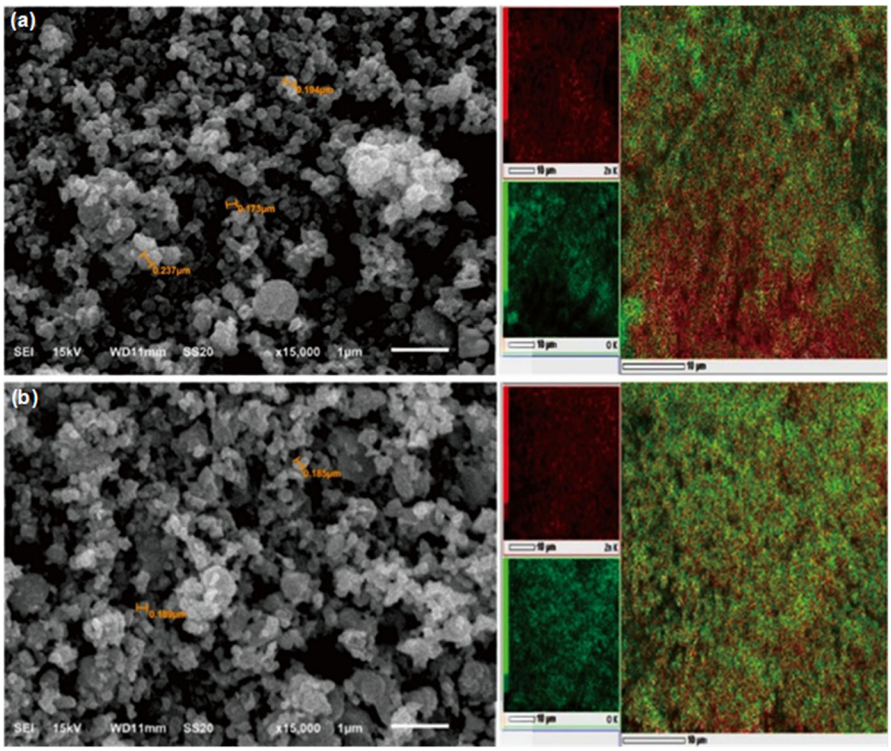


Fig 2. Particle size and element characterization using SEM-EDX with magnification of 15000× (a) ZnO-NPs and (b) ZnO-NPs HSFI-9

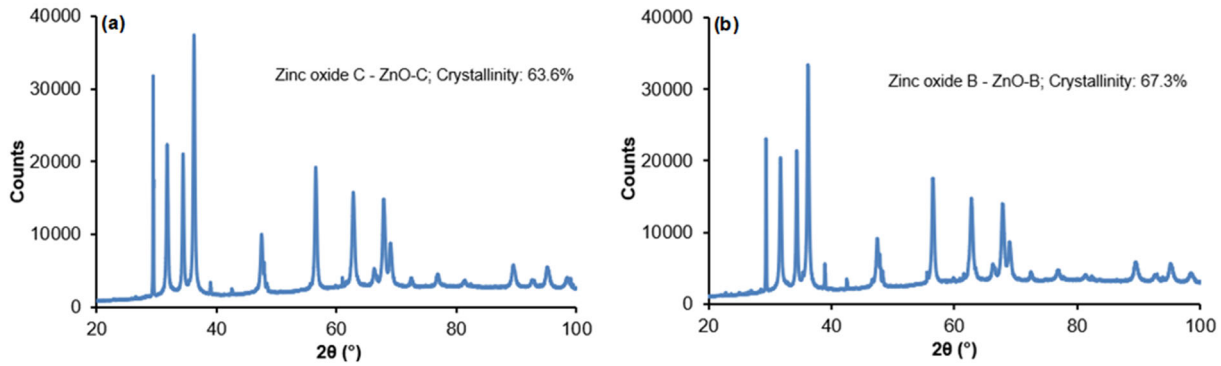


Fig 3. Diffraction spectral image of XRD: (a) ZnO-NPs, and (b) ZnO-NPs HSFI-9

Reported values of ZnO crystallinity in related studies typically reach around 60%, supporting the validity of the present findings [41]. Precise control of synthesis parameters, particularly pH (10.0) and temperature (60 °C) during the co-precipitation process, was essential for producing stable and homogeneous nanoparticles. However, potential risks related to pH or temperature instability, which could result in uneven precipitation or the formation of undesired by-products, should be carefully considered due to their possible influence on nanoparticle quality.

In terms of colloidal stability, the zeta potential measurements demonstrated that ZnO-NPs HSFI-9 exhibited a zeta potential value of approximately −29.01 mV ± 0.70, suggesting good dispersion and strong electrostatic stabilization in suspension. Conversely, conventional ZnO-NPs showed lower zeta potential values, which may be associated with the formation of particle aggregates. The higher zeta potential of ZnO-NPs HSFI-9 supports the improved stability and narrower size distribution observed, reinforcing the role of HSFI-9 extract in enhancing nanoparticle stability [42].

Altogether, these results confirm that precise control over synthesis parameters, including extract composition, pH, temperature, and mixing duration, is crucial for producing high-quality nanoparticles. Despite potential risks associated with extract handling and synthesis optimization, the obtained data indicate that ZnO-NPs HSFI-9 exhibit superior physicochemical characteristics compared with conventional ZnO-NPs, particularly in terms of reduced particle size, narrower distribution, and higher crystallinity.

In this study, ZnO-NP HSFI-9 activity was superior on Gram-positive *S. aureus* than on Gram-negative *K. pneumoniae*, *P. aeruginosa*, and *E. aerogenes*. However, the two ZnO-NPs were unable to detain the growth of Gram-positive *E. faecalis* and Gram-negative *A. baumannii*. This is contrary to research results, which stated good antibacterial activity of ZnO-NP with a particle size < 100 nm against *E. faecalis* [37], and also *A. baumannii* [43-44]. The relatively large particle size of ZnO-NPs in this study could be the excuse for its antibacterial inconsistency. In addition, the morphology of the ZnO-NP particles can also influence their antibacterial activity. Morphological forms resembling flowers are known to have the highest activity against *S. aureus* when compared with rod and spherical forms. The crystal morphology of ZnO-NPs influences the ease with which particles penetrate bacterial cell membranes [45].

The difference in ZnO-NPs particle size can be caused by the synthesis method. In this research, green synthesis was carried out using the precipitation method to avoid high production costs due to the use of expensive equipment, economic reasons, and fast processing [46]. The morphology of ZnO-NPs can also vary depending on the secondary metabolites that will be impregnated. Various types of microbial secondary metabolites impregnated with Zn nitrate can produce types of crystal morphology such as spherical, rod, cubic, triangular, and elongated [47]. In addition to crystal size and morphology, various parameters, such as precursor concentration, synthesis time, temperature, and pH, can also influence the biological activity of ZnO-NP. Alkaline pH is stated to be good for synthesis, which in this study was applied using NaOH for alkaline conditions of pH 10.0. Differences in pH cause the number of H^+ or OH^- ions to vary and ultimately can cause differences in the morphology of the NP-ZnO crystals formed [36].

The difference in particle sizes found in this study can be explained by the use of various measurement techniques. Different methods, both direct (SEM) and indirect (DLS), were employed to analyze the particle size. Although direct methods are generally considered more accurate, using a combination of several methods is recommended to ensure the validity of the results [48]. Measurements using DLS showed larger particle sizes, in the micrometer range (> 1000 nm), which contrasts with the general definition of nanoparticles, which are typically below 100 nm. This discrepancy can be attributed to particle aggregation occurring during the synthesis or measurement process, rather than the size of individual particles. DLS measures the hydrodynamic diameter, which includes the solvent layer surrounding the nanoparticles, resulting in larger measurements than techniques like SEM, which measure particle size based on physical morphology. The difference in size obtained from both techniques, DLS and SEM, is due to the fundamental differences in the measurement principles of each. Particle aggregation detected by DLS can lead to significant differences in size measurements compared to SEM, which measures individual particles. This aligns with the observed decrease in antibacterial activity in larger nanoparticles, likely due to aggregation, which limits the nanoparticles' ability to interact effectively with bacteria, reducing the antibacterial potential [49-50]. Another factor suspected to contribute to the larger size measurements obtained by DLS is that the scattered light intensity is directly proportional to the particle diameter raised to the sixth power, so larger particles have a greater impact on the intensity signal, even if few large particles are present. The polydispersity index indicates the variation in particle size, with a value close to 0 suggesting a more uniform size distribution, while higher values indicate a broader distribution [51-52]. The polydispersity index values for ZnO-NP and ZnO-NP HSFI-9 are greater than 0.4 (Table 2), indicating that the particle size distribution for both is polydisperse, making the interpretation of DLS particle size

measurements more complex [53]. Although SEM is more complex to use, it has the advantage of visually showing the particle size distribution more clearly compared to DLS [54]. In this study, the expected ZnO-NPs was within the 5–100 nm range, considering that previous studies have shown that nanoparticles in this size range have optimal antibacterial potential. However, DLS measurements showed larger sizes in the micrometer scale. Nevertheless, this size difference does not affect the validity of the results, as larger sizes do not necessarily reduce antibacterial effectiveness, especially when nanoparticles function in systems integrated with other components [55].

Other parameters, such as zeta potential, are useful to evaluate the electrokinetic potential of colloidal nanoparticle systems [56-57]. In this study, the zeta potential value of both ZnO-NPs was negative, which could be caused by the alkaline atmosphere of the colloid [58]. ZnO-NP HSFI-9 has a zeta potential of around −30 mV, which indicates the nanoparticle formed was stable and well dispersed in solution [58], while the zeta potential of ZnO-NP indicates the presence of agglomerated compounds [59-60]. Agglomeration in ZnO-NP can be caused by excessive physical sonication processes before reading the particle size using DLS. This agglomeration causes the surface energy to decrease and can have a negative impact if it cannot be controlled, for example, ZnO-NPs that experience agglomeration tend to be cytotoxic [61-62].

The degree of crystallinity from XRD examination results is also important for evaluating the diameter size and performance of nanoparticles. The degree of crystallinity can be influenced by the type of nanoparticle, preparation conditions, and precursor concentration. The percentage degree of crystallinity can decrease along with decreasing nanoparticle diameter, but in this study, the percentage degree of crystallinity of ZnO-NP HSFI-9 was higher than that of ZnO-NP, even though the particle size was smaller. Increasing the degree of crystallinity will increase the stiffness of the compound [39], and considered to increase their activity performance [40], which in this study was proven to increase the activity of ZnO-NP HSFI-9 as an antibacterial.

Dominant secondary metabolites in the ethyl acetate extract of *B. subtilis* subsp. *subtilis* HSFI-9 (Table 3), include surfactin (82.22%), 4-dodecylbenzenesulfonic acid (6.24%), β-muricholic acid (6.01%), corynebactin (1.62%), and myristyl sulfate (1.36%). Surfactin was identified in the chromatographic peak with retention times ranging from 20.84 to 22.31 min. The principal bioactive compounds in the HSFI-9 extract are surfactin and corynebactin. Surfactin, a cyclic lipopeptide produced by *Bacillus* species, is widely known for its antifungal and antibacterial properties [63]. Corynebactin, a catecholate siderophore with a molecular formula of $C_{39}H_{42}N_6O_{18}$ (MW ≈ 8.8×10^2), is synthesized by various *Bacillus* species such as *Bacillus velezensis* and *Bacillus halotolerans*. Corynebactin has demonstrated moderate antibacterial and cytotoxic activities [64-65]. Notably, previous studies have reported the incorporation of surfactin into nanoparticle formulations, where it exhibited antibiofilm activity against *P. aeruginosa* [66]. However, similar studies involving corynebactin are still lacking.

However, certain compounds detected in the extract, such as PFOA, triclocarban, and monobutyl phthalate, are likely contaminants that may have been introduced during the extraction process. These compounds are often associated with environmental pollutants or synthetic contaminants, and their presence in the extract does not necessarily reflect natural metabolites produced by *B. subtilis* subsp. *subtilis* HSFI-9. While these compounds were detected at low concentrations compared to the dominant metabolites, their presence raises concerns about potential contamination. This possibility should be addressed, and further investigations are necessary to determine the source of these contaminants and their potential influence on the biological activity of the extract [67-68].

The antibacterial activity of ZnO-NP HSFI-9, along with its particle size profile and crystal morphology, was evaluated. ZnO-NP HSFI-9 holds significant promise for development as an antibacterial agent, particularly for topical applications. Future studies should focus on optimizing methods to reduce

Table 3. Recapitulation of secondary metabolites of ethyl acetate extract of *B. subtilis* subsp. *subtilis* HSFI-9 profiled by targeted and non-targeted UHPLC-HRMS

Formula	Compound name	Molecular weight (MW)	Retention time (min)	%Area
$C_{10}H_{13}N_5O_4$	Adenosine	267	2.0	0.03
$C_{11}H_{13}NO3$	NP-008309	207	9.0	0.02
$C_{12}H_{12}N_2O_3$	NP-020292	232	9.0	0.01
$C_{39}H_{42}N_6O_{18}$	Corynebactin	882	9.2–11.2	1.62
$C_{26}H_{43}NO_6$	Glycocholic acid	465	12.0	0.57
$C_8H_8Cl_2N_2O$	Monomethyldiuron (DCPMU)	218	12.0	0.03
$C_1H_{30}O_4$	NP-001596	286	13.0	0.01
$C_{26}H_{45}NO_6S$	Taurochenodeoxycholic acid (sodium salt)	499	13.0	0.13
$C_{12}H_{22}O_4$	Dodecanedioic acid	230	13.0	0.01
$C_{18}H_{34}O_5$	(15*Z*)-9,12,13-Trihydroxy-15-octadecenoic acid	330	13.0	0.26
$C_{12}H_{14}O_4$	Monobutyl phthalate	222	13.0	0.01
$C_{24}H_{40}O_5$	β-Muricholic acid	408	13.0	6.01
$C_{26}H_{43}NO_5$	Glycochenodeoxycholic acid	449	14.0	0.70
$C_8HF_{15}O_2$	Perfluorooctanoic acid (PFOA)	414	14.0	0.13
$C_{14}H_{22}O_2$	2,5-di-*tert*-Butylhydroquinone	222	15.0	0.04
$C_{24}H_{40}O_4$	Deoxycholic acid	392	15.0	0.03
$C_{12}H_{26}O_4S$	Dodecyl sulfate	266	16.0	0.52
$C_{14}H_{30}O_4S$	Myristyl sulfate	294	17.0	1.36
$C_{18}H_{30}O_3S$	4-Dodecylbenzenesulfonic acid	326	17.0	6.24
$C_{13}H_9Cl_3N_2O$	Triclocarban	314	18.0	0.02
$C_{15}H_{22}O_3$	NP-002089	250	19.0	0.02
$C_{16}H_{32}O_3$	16-Hydroxyhexadecanoic acid	272	19.0	0.01
$C_{53}H_{93}N_7O_{13}$	Surfactin C	1036	20.8–22.3	82.22

the particle size of ZnO-NP HSFI-9. Additionally, it is essential to explore the antibacterial mechanism of ZnO-NP HSFI-9, given the observed variability in its antibacterial activity across different studies. The development of appropriate topical formulations, such as gels, ointments, or creams, should also be considered for subsequent pre-clinical *in vivo* applications.

■ CONCLUSION

ZnO-NP HSFI-9 demonstrates antibacterial activity against *S. aureus*, *K. pneumoniae*, and *E. aerogenes*. The particle size of ZnO-NP HSFI-9 was assessed in the nanometer range through SEM-EDX analysis, while the particle size distribution and crystal morphology were thoroughly evaluated using XRD analysis. Although ZnO-NP HSFI-9 shows promise as an antibacterial agent, its effectiveness is influenced by particle aggregation and inconsistent antibacterial performance across different bacterial strains. Therefore, further optimization of the synthesis method and formulation is necessary to enhance particle stability and ensure more consistent antibacterial activity.

■ ACKNOWLEDGMENTS

This research was funded by the *Direktorat Riset, Teknologi, dan Pengabdian kepada Masyarakat* (DRTPM) Ministry of Education, Culture, Research and Technology using regular fundamental research scheme with contract number of 108/E5/PG.02.00.PL/2024, derivative contract number of 022/LL6/PB/AL.04/2024; 003/061026/PB/SP2H/AK.04/2024.

■ CONFLICT OF INTEREST

The authors declared no conflict of interest.

■ AUTHOR CONTRIBUTIONS

The research concept and study design were developed by Maya Dian Rakhmawatie, Nur Fadhila Sari, Mazidatu Khoirinnisa Adiyanti, and Arman Suryani. Data collection, as well as data analysis and interpretation, were carried out by Maya Dian Rakhmawatie, Nur Fadhila Sari, Mazidatu Khoirinnisa Adiyanti, and Arman Suryani. The initial manuscript draft, critical revision of the scientific content, and final approval of the manuscript were performed by Maya Dian Rakhmawatie, Ana Hidayati Mukaromah, Ika Dyah Kurniati, and Arman Suryani. Statistical analyses were conducted by Maya Dian Rakhmawatie, Nur Fadhila Sari, Mazidatu Khoirinnisa Adiyanti, and Arman Suryani. Administrative, technical, and material support, as well as research supervision, were provided by Maya Dian Rakhmawatie, Ana Hidayati Mukaromah, Ika Dyah Kurniati, and Arman Suryani.

■ REFERENCES

[1] Rakhmawatie, M.D., Marfu'Ati, N., Barsaliputri, B., Fikriyah, A.Z., and Ethica, S.N., 2023, Antibacterial activity and GC-MS profile of secondary metabolites of *Bacillus subtilis* subsp. *subtilis* HSFI-9 associated with *Holothuria scabra*, *Biodiversitas*, 24 (5), 2843–2849.

[2] Rakhmawatie, M.D., Wibawa, T., Lisdiyanti, P., Pratiwi, W.R., Damayanti, E., and Mustofa, M., 2021, Potential secondary metabolite from Indonesian Actinobacteria (InaCC A758) against *Mycobacterium tuberculosis*, *Iran. J. Basic Med. Sci.*, 24 (8), 1058–1068.

[3] Ozdal, M., and Gurkok, S., 2022, A Recent advances in nanoparticles as antibacterial agent, *ADMET DMPK*, 10 (2), 115–129.

[4] Yılmaz, G.E., Göktürk, I., Ovezova, M., Yılmaz, F., Kılıç, S., and Denizli, A., 2023, Antimicrobial nanomaterials: A review, *Hygiene*, 3 (3), 269–290.

[5] Chabib, L., Hidayat, A.M.U.J., Trianloka, A.M.B., Pangestu, M.I., Suryani, A., and Yulianto, Y., 2021, Therapeutic potential of *Cymbopogon schoenanthus* (L.) developed into nanoparticle technology, *Pharm. Educ.*, 21 (2), 210–214.

[6] Chabib, L., Suryani, A., Hakim, S.N.P., Rizki, M.I., Firmansyah, F., Yulianto, Y., and Romadhonsyah, F., 2022, *Stevia rebaudiana* as a nutraceutical for COVID-19 patients with no sugar diet during recovery and its nanoparticle application, *Pharm. Educ.*, 22 (2), 174–179.

[7] Gudkov, S.V., Burmistrov, D.E., Serov, D.A., Rebezov, M.B., Semenova, A.A., and Lisitsyn, A.B., 2021, A mini review of antibacterial properties of ZnO nanoparticles, *Front. Phys.*, 9, 641481.

[8] Martínez-Carmona, M., Gun'ko, Y., and Vallet-Regí, M., 2018, ZnO nanostructures for drug delivery and theranostic applications, *Nanomaterials*, 8 (4), 268.

[9] Viswanathan, K., Vaiyamalai, R., Bharathi Babu, D., Mala Priyadharshini, M.L., Raman, M., and Dhinakarraj, G., 2018, Ketoconazole-conjugated ZnO nanoparticles based semi-solid formulation and study their impacts on skin disease, *IET Nanobiotechnol.*, 12 (8), 1097–1101.

[10] Rahman, H.S., Othman, H.H., Abdullah, R., Edin, H.Y.A.S., and AL-Haj, N.A., 2022, Beneficial and toxicological aspects of zinc oxide nanoparticles in animals, *Vet. Med. Sci.*, 8 (4), 1769–1779.

[11] Gautam, R., Yang, S., Maharjan, A., Jo, J., Acharya, M., Heo, Y., and Kim, C.Y., 2021, Prediction of skin sensitization potential of silver and zinc oxide nanoparticles through the human cell line activation test, *Front. Toxicol.*, 3, 649666.

[12] Herrera Pérez, G.M., Castellano, L.E., and Ramírez Valdespino, C.A., 2024, *Trichoderma* and mycosynthesis of metal nanoparticles: Role of their secondary metabolites, *J. Fungi*, 10 (7), 443.

[13] Singh, N.A., Narang, J., Garg, D., Jain, V., Payasi, D., Suleman, S., and Swami, R.K., 2023, Nanoparticles synthesis via microorganisms and their prospective applications in agriculture, *Plant Nano Biol.*, 5, 100047.

[14] El-Ghwas, D.E., 2022, Characterization and biological synthesis of zinc oxide nanoparticles by new strain of *Bacillus foraminis*, *Biodiversitas*, 23 (1), 548–553.

[15] Sabir, S., Zahoor, M.A., Waseem, M., Siddique, M.H., Shafique, M., Imran, M., Hayat, S., Malik, I.R., and Muzammil, S., 2020, Biosynthesis of ZnO

nanoparticles using *Bacillus subtilis*: Characterization and nutritive significance for promoting plant growth in *Zea mays* L, *Dose-Response*, 18 (3), 1559325820958911.

[16] Rehman, S., Jermy, B.R., Akhtar, S., Borgio, J.F., Abdul Azeez, S., Ravinayagam, V., Al Jindan, R., Alsalem, Z.H., Buhameid, A., and Gani, A., 2019, Isolation and characterization of a novel thermophile; *Bacillus haynesii*, applied for the green synthesis of ZnO nanoparticles, *Artif. Cells, Nanomed., Biotechnol.*, 47 (1), 2072–2082.

[17] Vale de Macedo, G.H.R., Costa, G.D.E., Oliveira, E.R., Damasceno, G.D., Mendonça, J.S.P., Silva, L.D.S., Chagas, V.L., Bazán, J.M.N., Aliança, A.S.D.S., de Miranda, R.D.C.M., Zagmignan, A., de Souza Monteiro, A., and Nascimento da Silva, L.C., 2021, Interplay between ESKAPE pathogens and immunity in skin infections: An overview of the major determinants of virulence and antibiotic resistance, *Pathogens*, 10 (2), 148.

[18] Rohani, R., Dzulkharnien, N.S.F., Harun, N.H., and Ilias, I.A., 2022, Green approaches, potentials, and applications of zinc oxide nanoparticles in surface coatings and films, *Bioinorg. Chem. Appl.*, 2022 (1), 3077747.

[19] Hajos, M., Starowicz, M., Brzychczyk, B., Basista, G., and Francik, S., 2025, Size distribution of zinc oxide nanoparticles depending on the temperature of electrochemical synthesis, *Materials*, 18 (2), 458.

[20] Susanti, D., Haris, M.S., Taher, M., and Khotib, J., 2022, Natural products-based metallic nanoparticles as antimicrobial agents, *Front. Pharmacol.*, 13, 895616.

[21] Silvia, R., Wahyuni, W.T., Rohaeti, E., Aisyah, S., Septaningsih, D.A., Karomah, A.H., and Rafi, M., 2024, LC-HRMS-based metabolomics approach reveals antioxidant compounds from *Centella asiatica* leaves extracts, *Indones. J. Chem.*, 24 (6), 1861–1869.

[22] Khan, M.F., Ansari, A.H., Hameedullah, M., Ahmad, E., Husain, F.M., Zia, Q., Baig, U., Zaheer, M.R., Alam, M.M., Khan, A.M., AlOthman, Z.A., Ahmad, I., Md Ashraf, G., and Aliev, G., 2016, Sol-gel synthesis of thorn-like ZnO nanoparticles endorsing mechanical stirring effect and their antimicrobial activities: Potential role as nano-antibiotics, *Sci. Rep.*, 6 (1), 27689.

[23] Suciyati, S.W., Manurung, P., Junaidi, J., and Situmeang, R., 2024, Optical and crystal structure properties of ZnO nanoparticle synthesized through biosynthesis method for photocatalysis application, *Indones. J. Chem.*, 24 (1), 125–140.

[24] Ashraf, R., Riaz, S., Hussain, S.S., and Naseem, S., 2015, Effect of pH on properties of ZnO nanoparticles, *Mater. Today: Proc.*, 2 (10, Pt. B), 5754–5759.

[25] Khan, A., Miller, W.R., Axell-House, D., Munita, J.M., and Arias, C.A., 2022, Antimicrobial susceptibility testing for enterococci, *J. Clin. Microbiol.*, 60 (9), e00843–21.

[26] Endo, S., Tada, T., Oshiro, S., Hishinuma, T., Tohya, M., Watanabe, S., Sekiguchi, J.I., Abe, M., Nakada, K., and Kirikae, T., 2024, Evaluation of antimicrobial susceptibility tests for *Acinetobacter* and *Pseudomonas* species using disks containing a high dose of meropenem, *Sci. Rep.*, 14 (1), 2749.

[27] Yadav, B.C., Singh, S., and Yadav, T.P., 2015, Titania prepared by ball milling: Its characterization and application as liquefied petroleum gas sensor, *Synth. React. Inorg., Met.-Org., Nano-Met. Chem.*, 45 (4), 487–494.

[28] El-Beltagi, H.S., Ragab, M., Osman, A., El-Masry, R.A., Alwutayd, K.M., Althagafi, H., Alqahtani, L.S., Alazragi, R.S., Alhajri, A.H., and El-Saber, M.M., 2024, Biosynthesis of zinc oxide nanoparticles *via* neem extract and their anticancer and antibacterial activities, *PeerJ*, 12, e17588.

[29] Suryani, A., Chabib, L., Fitria, A., Nurlina, S., and Kartika, E.R., 2025, Peppermint essential oil nanoliposomes: Innovative formulation for effective hair growth, *J. Appl. Pharm. Sci.*, 15 (6), 178–189.

[30] Adlan, R.H., Mustafa, J.Y., and Faja, O.M., 2022, Green synthesis of ZnO nanoparticles using pomegranate fruit extract, *J. Pharm. Negat. Results*, 13 (8), 456–467.

[31] Suryani, A.E., Nisa, K., Handayani, S., Darsih, C., Wuryastuty, H., and Yanuartono, Y., 2025, The UHPLC-HRMS profiling, *in vitro*-antioxidant and pancreatic lipase inhibitory activities of *Peronema canescens* leaves extract and fractions from Indonesia, *J. Appl. Pharm. Sci*., 15 (5), 75–89.

[32] Zare-Zardini, H., Alizadeh, A., Saberian, E., Jenča, A., Jenca, A., Petrášová, A., Jenčová, J., Hasani, S.T., Heidari, M.A., and Sahraei, N., 2025, Enhanced antimicrobial efficacy and biocompatibility of albumin nanoparticles loaded with *Mentha* extract against methicillin resistant *Staphylococcus aureus*, *Sci. Rep*., 15 (1), 6548.

[33] Gutiérrez-Pinzón, Y., Martínez-Preciado, A.H., Velázquez-López, J.M., Pech-Jiménez, C., Zúñiga-Mayo, V.M., Guevara-Martínez, S.J., and Velázquez-Juárez, G., 2025, Antimicrobial potential of nanomaterials synthesized with extracts from annona plants: A review, *Antibiotics*, 14 (8), 748.

[34] Kourmouli, A., Valenti, M., van Rijn, E., Beaumont, H.J.E., Kalantzi, O.I., Schmidt-Ott, A., and Biskos, G., 2018, Can disc diffusion susceptibility tests assess the antimicrobial activity of engineered nanoparticles?, *J. Nanopart. Res*., 20 (3), 62.

[35] Zhang, X., Hou, X., Ma, L., Shi, Y., Zhang, D., and Qu, K., 2023, Analytical methods for assessing antimicrobial activity of nanomaterials in complex media: Advances, challenges, and perspectives, *J. Nanobiotechnol*., 21 (1), 97.

[36] Xu, J., Huang, Y., Zhu, S., Abbes, N., Jing, X., and Zhang, L., 2021, A review of the green synthesis of ZnO nanoparticles using plant extracts and their prospects for application in antibacterial textiles, *J. Eng. Fibers Fabr.*, 16, 15589250211046242.

[37] Djearamane, S., Loh, Z.C., Lee, J.J., Wong, L.S., Rajamani, R.K., Luque, P.A., Gupta, P.K., and Liang, S.X.T., 2022, Remedial aspect of zinc oxide nanoparticles against *Serratia marcescens* and *Enterococcus faecalis*, *Front. Pharmacol.*, 13, 891304.

[38] Sun, P., Lv, Z., and Sun, C., 2024, Study on the synthesis of nano zinc oxide particles under supercritical hydrothermal conditions, *Nanomaterials*, 14 (10), 844.

[39] Niyom, Y., Phakkeeree, T., Flood, A., and Crespy, D., 2019, Synergy between polymer crystallinity and nanoparticles size for payloads release, *J. Colloid Interface Sci.*, 550, 139–146.

[40] Sanusi, O.M., Benelfellah, A., Bikiaris, D.N., and Aït Hocine, N., 2021, Effect of rigid nanoparticles and preparation techniques on the performances of poly(lactic acid) nanocomposites: A review, *Polym. Adv. Technol.*, 32 (2), 444–460.

[41] Isfa, B., Jamarun, N., Emriadi, E., Arief, S., Ritonga, A.H., Tanjung, D.A., and Sisca, V., 2023, Characterization and application of TiO_2/ZnO nanoparticles as pigments in matt-type water-based paint, *Int. J. Technol.*, 14 (2), 291–319.

[42] Suryani, A., Istiqhfarin, H.A.S., Hidayah, N., Nitisara, N.N., Aryanti, A.M., Ardana, R., and Kartika, E.R., 2025, Synergistic modification of polyvinyl alcohol and natural phospholipids: Nanoliposomal carrier for *Sonneratia caseolaris* L. delivery and therapeutic care, *J. Appl. Pharm. Sci*., 15 (12), 251–265.

[43] Tiwari, V., Mishra, N., Gadani, K., Solanki, P.S., Shah, N.A., and Tiwari, M., 2018, Mechanism of anti-bacterial activity of zinc oxide nanoparticle against carbapenem-resistant *Acinetobacter baumannii*, *Front. Microbiol.*, 9, 1218.

[44] Marques, G.N., Moreira, A.J., Nóbrega, E.T.D., Braga, S., Argentin, M.N., da Cunha Camargo, I.L.B., Azevedo, E., Pereira, E.C., Bernardi, M.I.B., and Mascaro, L.H., 2024, Selective inhibitory activity of multidrug-resistant bacteria by zinc oxide nanoparticles, *J. Environ. Chem. Eng.*, 12 (1), 111870.

[45] Sirelkhatim, A., Mahmud, S., Seeni, A., Kaus, N.H.M., Ann, L.C., Bakhori, S.K.M., Hasan, H., and Mohamad, D., 2015, Review on zinc oxide nanoparticles: Antibacterial activity and toxicity mechanism, *Nano-Micro Lett.*, 7 (3), 219–242.

[46] Zhou, X.Q., Hayat, Z., Zhang, D.D., Li, M.Y., Hu, S., Wu, Q., Cao, Y.F., and Yuan, Y., 2023, Zinc oxide nanoparticles: Synthesis, characterization, modification, and applications in food and agriculture, *Processes*, 11 (4), 1193.

[47] Huq, M.A., Apu, M.A.I., Ashrafudoulla, M., Rahman, M.M., Parvez, M.A.K., Balusamy, S.R.,

Akter, S., and Rahman, M.S., 2023, Bioactive ZnO nanoparticles: Biosynthesis, characterization and potential antimicrobial applications, *Pharmaceutics*, 15 (11), 2634.

[48] Caputo, F., Clogston, J., Calzolai, L., Rösslein, M., and Prina-Mello, A., 2019, Measuring particle size distribution of nanoparticle enabled medicinal products, the joint view of EUNCL and NCI-NCL. A step by step approach combining orthogonal measurements with increasing complexity, *J. Controlled Release*, 299, 31–43.

[49] Eaton, P., Quaresma, P., Soares, C., Neves, C., de Almeida, M.P., Pereira, E., and West, P., 2017, A direct comparison of experimental methods to measure dimensions of synthetic nanoparticles, *Ultramicroscopy*, 182, 179–190.

[50] Norouzi, N., Ong, Y., Damle, V.G., Habibi Najafi, M.B., and Schirhagl, R., 2020, Effect of medium and aggregation on antibacterial activity of nanodiamonds, *Mater. Sci. Eng., C*, 112, 110930.

[51] Suryani, A., Laksitorini, M.D., and Sulaiman, T.N.S., 2024, Ferrous fumarate nanoliposomes: Formulation, characterization, and diffusion profiles, *J. Appl. Pharm. Sci*., 14 (5), 157–165.

[52] Suryani, A., Suwarno, A.S., Parawansa, P., Puspita, I., Audrelia, J.K., and Qumayroh, A.A., 2026, Nanoparticles PLGA-chitosan/Na-alginate as a base for *Zanthoxylum acanthopodium* fruit extracts delivery and care as antimalarials, *J. Appl. Pharm. Sci*., 16 (3), 236–249.

[53] Teulon, J.M., Godon, C., Chantalat, L., Moriscot, C., Cambedouzou, J., Odorico, M., Ravaux, J., Podor, R., Gerdil, A., Habert, A., Herlin-Boime, N., Chen, S.W., and Pellequer, J.L., 2019, On the operational aspects of measuring nanoparticle sizes, *Nanomaterials*, 9 (1), 18.

[54] Takechi-Haraya, Y., Ohgita, T., Demizu, Y., Saito, H., Izutsu, K., and Sakai-Kato, K., 2022, Current status and challenges of analytical methods for evaluation of size and surface modification of nanoparticle-based drug formulations, *AAPS PharmSciTech*, 23 (5), 150.

[55] Iskakova, Z., Kozhantayeva, A., Temirbekova, A., Mukhtubayeva, S., Bissenova, G., Tekebayeva, Z., Almagambetov, K., Tashenov, Y., and Sarmurzina, Z., 2025, Green synthesis of silver nanoparticles using *Circaea lutetiana* ethanolic extract: Phytochemical profiling, characterization, and antimicrobial evaluation, *Int. J. Mol. Sci.*, 26 (12), 5505.

[56] Chabib, L., Ar Rodli, F.H., Nugroho, B.H., Suryani, A., and Firmansyah, F., 2024, Development of nanoliposome formulation of beta-carotene using high speed homogeniser method, *Pharm. Educ*., 24 (2), 1–8.

[57] Suryani, A., Affani, A.R., Safitri, B.W., Azis, I.A., Aldo, M.F.E., and Sofia, H., 2025, Innovative formulation of solid lipid nanoparticle loaded with carrot seed essential oil for potential antioxidant activity and sun protection, *Trop. J. Nat. Prod. Res*., 9 (12), 6239–6248.

[58] Trianloka, B.A.M., Chabib, L., Maharani, W.H.P., Fitria, A., Ramadani, A.P., Suryani, A., and Firmansyah, F., 2025, Enhancing hair follicle stimulation: A nanoliposome-based delivery of lavender essential oil (*Lavandula angustifolia* Mill.), *Trop. J. Nat. Prod. Res.*, 9 (8), 3687–3694

[59] Flemban, T.H., 2023, Synthesis, characterization, and analysis of zinc oxide nanoparticles using varying pulsed laser ablation energies in liquid, *J. Exp. Nanosci.*, 18 (1), 2175817.

[60] Babu Boppudi, H., Subba Rao, Y., Kuchi, C., Ramesh Babu, A., Govinda, V., Jagadeesh, M., and Lavanya, M., 2023, Zinc oxide nanoparticles as an efficient antioxidant, photocatalyst, and heterogeneous catalyst in C–P bond synthesis, *Results Chem.*, 6, 101227.

[61] Shrestha, S., Wang, B., and Dutta, P., 2020, Nanoparticle processing: Understanding and controlling aggregation, *Adv. Colloid Interface Sci.*, 279, 102162.

[62] Khan, A.U.H., Liu, Y., Naidu, R., Fang, C., Dharmarajan, R., and Shon, H., 2021, Interactions between zinc oxide nanoparticles and

hexabromocyclododecane in simulated waters, *Environ. Technol. Innovation*, 24, 102078.

[63] Iqbal, S., Begum, F., Rabaan, A.A., Aljeldah, M., Al Shammari, B.R., Alawfi, A., Alshengeti, A., Sulaiman, T., and Khan, A., 2023, Classification and multifaceted potential of secondary metabolites produced by *Bacillus subtilis* group: A comprehensive review, *Molecules*, 28 (3), 927.

[64] Nifakos, K., Tsalgatidou, P.C., Thomloudi, E.E., Skagia, A., Kotopoulis, D., Baira, E., Delis, C., Papadimitriou, K., Markellou, E., Venieraki, A., and Katinakis, P., 2021, Genomic analysis and secondary metabolites production of the endophytic *Bacillus velezensis* Bvel1: A biocontrol agent against *Botrytis cinerea* causing bunch rot in post-harvest table grapes, *Plants*, 10 (8), 1716.

[65] Tkachuk, N., Zelena, L., Lukash, O., and Mazur, P., 2021, Microbiological and genetic characteristics of *Bacillus velezensis* bacillibactinproducing strains and their effect on the sulfate-reducing bacteria biofilms on the poly(ethylene terephthalate) surface, *Ecol. Quest.*, 32 (2), 119–129.

[66] Rahman, L., Sarwar, Y., Khaliq, S., Inayatullah, I., Abbas, W., Mobeen, A., Ullah, A., Hussain, S.Z., Khan, W.S., Kyriazi, M.E., Hussain, I., Kanaras, A.G., and Rehman, A., 2023, Surfactin-conjugated silver nanoparticles as an antibacterial and antibiofilm agent against *Pseudomonas aeruginosa*, *ACS Appl. Mater. Interfaces*, 15 (37), 43321–43331.

[67] Han, Y., Wang, J., Zhao, Q., Xie, X., Song, R., Xiao, Y., Kang, X., Zhang, L., Zhang, Y., Peng, C., and You, Z., 2020, Pioglitazone alleviates maternal sleep deprivation-induced cognitive deficits in male rat offspring by enhancing microglia-mediated neurogenesis, *Brain, Behav., Immun.*, 87, 568–578.

[68] Giuliani, A., Zuccarini, M., Cichelli, A., Khan, H., and Reale, M., 2020, Critical review on the presence of phthalates in food and evidence of their biological impact, *Int. J. Environ. Res. Public Health*, 17 (16), 5655.